



# On the variability of motor-evoked potentials: experimental results and mathematical model

Charles Capaday<sup>1</sup>

Received: 13 February 2021 / Accepted: 1 July 2021 / Published online: 29 July 2021  
© The Author(s), under exclusive licence to Springer-Verlag GmbH Germany, part of Springer Nature 2021

## Abstract

The purpose of this study was to determine the form of the relation between the mean amplitude and variance of motor-evoked potentials (MEP). To this end, single-pulse transcranial magnetic stimulation (TMS) was applied over the motor cortex of seventeen neurologically normal adult human subjects. The coil was positioned at a locus on the scalp that elicited an MEP in the first dorsal interosseous (FDI) at the lowest stimulus intensity. The subjects were instructed to maintain tonic activity in the FDI of 5 or 10% of the maximum voluntary contraction (MVC). The relation between MEP variance and amplitude was found to have an inverted parabolic shape, with maximal variance occurring near the half-maximal MEP amplitude. The coefficient of variation CV of MEPs decreased approximately as a rectangular hyperbolic function of MEP amplitude (i.e.  $\sim 1/\text{MEP}$ ). A probabilistic model is proposed to explain the inverted parabolic relation between MEP variance and MEP amplitude, as well as the sigmoid shape of the MEP input–output relation (i.e. stimulus–response curve). The model is based on a description of  $\alpha$ -motoneurons as binary threshold units, with unit thresholds distributed according to a positively skewed probability density function. The units are driven by noisy synaptic input currents having a Gaussian distribution. The model predicts an inverse parabolic relation between MEP variance and amplitude and a sigmoid input–output relation, as experimentally observed. Furthermore, increasing model motoneuron excitability by increasing the background synaptic drive increases MEP variability independently of MEP size, a surprising prediction. The model also explains the approximately rectangular hyperbolic relation between CV and MEP amplitude. The implications of these results for the interpretation of neurophysiological experiments and the statistical analysis of MEPs are discussed.

**Keywords** Motor-evoked potential (MEP) · Transcranial magnetic stimulation (TMS) · Brain stimulation · MEP variance · Input–output curve

## Introduction

The input–output (recruitment) curves of monosynaptic reflexes (MSR) and MEPs are a sigmoid functions of stimulus intensity (Devanne et al. 1997; Hunt 1955; Rall 1955a). The variance of MSRs as a function of their amplitude can be described by an inverted parabola (Rudomin and Dutton 1969; Rudomin 1980). The relation between MEP variance and amplitude, however, has not been determined.

Knowledge of this relation is important for the interpretation of neurophysiological experiments and their statistical analysis. The form of these curves and how they change with the level of  $\alpha$ -motoneuron drive have yet to be explained in neurophysiological and mathematical terms. Although Rall has formulated a probability theory-based graphical model (Rall 1955b) and Capaday (1997) formulated an empirical graphical model, neither addresses the stated issues conjointly. Relatedly, the coefficient of variation CV of MEPs is inversely proportional to amplitude (e.g. Capaday et al. 1999; Darling et al. 2006; Devanne et al. 1997; Klein-Flugge et al. 2013), but the proper mathematical description of this relation and its neurophysiological basis remain to be established. Moreover, Darling et al. (2006) reported that the CV of MEPs was lower when subjects maintained tonic motor activity compared to rest. It is unclear, however, if the CV is in fact independent of MEP amplitude, per se. That is, do

---

Communicated by Winston D. Byblow.

✉ Charles Capaday  
charles.capaday@ccapcable.com

<sup>1</sup> Department of Health and Human Physiology, Motor Control Laboratories, University of Iowa, Iowa City, IA 52242, USA

MEPs of equal size obtained, respectively, at rest or superimposed on tonic background activity have the same CV.

To these ends, experiments were done to determine the relation between MEP amplitude and variance, as well as to characterize in detail the relation between MEP amplitude and CV. These will be referred to, respectively, as the Var–amplitude relation and the CV–amplitude relation. It will be shown that the Var–amplitude relation is described by an inverted parabola and that the CV–amplitude relation resembles a rectangular hyperbola of the form  $1/\text{MEP}$ . To explain these results, a minimal mathematical model based on basic neurophysiological variables was developed. The model includes a description of  $\alpha$ -motoneurons as binary threshold units, with unit threshold currents distributed according to a positively skewed probability density function. The units are driven by Gaussian synaptic input currents. It is also shown that MEP amplitude distribution histograms change with stimulus intensity and are not described by any obvious probability density function, a result also explained by the model. The implications of these results for the interpretation of neurophysiological experiments and the statistical analysis of MEPs are dealt with in the discussion. For example, the non-Gaussian statistics of MEPs place limit on tests of significance and curve-fitting algorithms.

## Materials and methods

### Subjects

Experiments were done on 17 healthy subjects (11 males, 6 females) ranging between 18 and 60 years. All subjects participated with their informed consent in accordance with the Declaration of Helsinki. The experiments were done at Université Laval where the author was on faculty at the time and approved by the local ethics committee.

### Electromyographic recordings and magnetic stimulation

The electromyogram (EMG) was recorded from the first dorsal interosseous (FDI) using a pair of surface Ag–AgCl disc electrodes (recording diameter 1 mm, separation  $\sim$  1 cm) placed over the belly of the muscle. Recordings were made from either the left or right FDI, depending on the subject's stated hand dominance. Only two subjects self-described themselves as left-handed. The electrodes were attached to the skin by O-shaped rings of double-sided adhesive film and further secured by a strip of tape. The electrodes were shielded right up to the recording surfaces and connected to an optically isolated preamplifier by a shielded twisted-pair cable. The shielded twisted-pair cable reduces magnetic interference from the stimulating coil. The reference

electrode, a large metal plate (3 cm  $\times$  9 cm) covered in gauze and moistened with saline, was placed high on the subject's arm on the side of the recordings and connected to the common input of the preamplifiers. The EMG signals were amplified, high-pass filtered at 20 Hz and low-pass filtered at 1 kHz prior to sampling (4 kHz) by an analogue-to-digital converter (A/D). The same EMG signals were also rectified and filtered (20–100 Hz) for sampling by a separate A/D converter channel. Magnetic stimuli were applied over the scalp using a Cadwell MES-10 electromagnetic stimulator, of maximum magnetic field strength 2 T, with a coned, double-D-shaped, focal coil. Each D-shaped wing of the coil was 7 cm long and 8 cm wide. The coil was shielded with a conductive epoxy (Nickel Print, GC electronics), insulated with electrical tape and the conductive coating grounded, resulting in little or no stimulus artefact.

### Experimental procedures

The coil was placed in contact with the scalp with the long axis of the intersection of its two loops pointing forwards and the coil handle backwards. To activate the FDI muscle, the coil was placed parallel to the sagittal midline and its mid-point was aligned antero-posteriorly at C3 or C4. Fine adjustments of coil position were made at the beginning of the experiments to identify the optimal location for each subject. Surface markings were then drawn on the scalp to serve as a reference grid against which the coil was positioned. The coil was maintained on the head by the experimenter and its position and orientation relative to the reference grid were constantly checked during the experiment. The inter-stimulus interval (ISI) varied randomly with a uniform distribution between 3 and 5 s. These intervals were used to minimize fatigue in these protracted experiments. Time series analysis of MEP amplitude records shows that the autocorrelation function decays to non-significant levels within an interval of three seconds, or less. Stimulus intensity was measured as a percentage of the maximum current which could be discharged through the coil.

Subjects sat in a chair and faced an analogue meter placed 1 m in front of them. The meter was calibrated so that a full-scale deflection of the needle corresponded to the maximum sustained isometric contraction of the muscle, as measured by the rectified and filtered (bandpass 10–20 Hz) surface electromyogram. The subject's right (or left) forearm rested on a table in the prone position with the distal joint of the index finger placed in a mould attached to a rigid stop. The experimental procedure required the subject to exert a prescribed level of FDI tonic activity, either 5% or 10% of MVC, depending on which level each subject was more comfortable maintaining. With background tonic activity, one can at least be sure of the subject's state with respect to at least motoneuron pool excitability at the time of the MEP.

The motor cortex was activated with magnetic stimuli during tonic contraction. The usual procedure was to increase the stimulus intensity starting at a value about 5–10% below threshold and increasing it in steps of 2–4% until saturation of the MEP amplitude. In some cases, the stimulus strength varied randomly. At each stimulus intensity, at least 8 stimuli were delivered to the motor cortex and the MEPs averaged and displayed in real time. The variance and CV of the elicited MEPs were also calculated in real time and stored for further analysis.

Five subjects were used to determine the amplitude distribution histogram of MEPs at two stimulus intensities, one near the active motor threshold (AMT) and the other near the  $S_{50}$  value. Subjects were asked to maintain a tonic level of background EMG activity in the FDI of either 5% or 10% of MVC, whilst TMS was applied to the scalp at random equiprobable intervals of between 3 and 5 s. Typically 64 consecutive MEPs were elicited in these experiments. In one case, 128 MEPs were elicited, with a brief rest period halfway. As repeated stimulation at maximal intensity was not well tolerated, no amplitude histograms were obtained for near maximal intensities.

### Data analysis and statistics

At each stimulus intensity and contraction level, the rectified and unrectified MEPs were averaged over a time segment of 250 ms, including 50 ms prior to the stimulus. As the MEP recordings were essentially artefact-free, the mean level of background EMG activity was measured in the 15–20 ms interval before the onset of the MEP, not before the stimulus. This provides a true measure of the background EMG level upon which the MEP occurs. The peak-to-peak (p–p) values of the averaged responses were measured and plotted against the stimulus intensity. The Boltzmann sigmoid function (Devanne et al. 1997) was used to fit the data points. The function relates the amplitude of the response MEP to the stimulus intensity  $S$  and is given by,

$$MEP(S) = \frac{MEP_{max}}{1 + e^{(S_{50}-S)/k}}, \tag{1}$$

where  $MEP_{max}$  is the maximum value or plateau of the relation,  $S_{50}$  is the stimulus intensity required to obtain a response 50% of the maximum ( $MEP_{1/2}$ ), and  $k$  is the slope parameter. The inverse of the slope parameter  $1/k$  is directly proportional to the maximal steepness of the function, which occurs at  $S_{50}$  and has a value of  $MEP_{max}/4k$ . Note that in normalized form  $MEP(S)/MEP_{max}$ , Eq. 1 can be interpreted as a measure of the level of motoneuron pool recruitment, as will be discussed. The Levenberg–Marquard nonlinear least-mean-squares algorithm was used to fit Boltzmann function to the data points (Press et al. 1986). Further details on the

Boltzmann equation can be obtained from previous publications of this laboratory (Capaday et al. 1999; Devanne et al. 1997; Kouchtir-Devanne et al. 2012). The variance of the average MEP at each stimulus intensity was calculated from the p–p amplitudes of the individual responses.

The data of the MEP amplitude distribution histogram experiments were analysed as follows. The histograms were constructed by binning MEP amplitudes (twenty bins) and the mean and variance of the distribution were calculated for each case. To determine whether the fluctuations of MEP amplitude from stimulus to stimulus were due to fluctuations of the background level of voluntary EMG activity, a linear regression analysis of MEP amplitude vs. mean background EMG was done for each case. The background EMG level was measured in the brief 20 ms interval between stimulus delivery and MEP onset. Such a near instantaneous measure is possible in recording conditions with little or no stimulus artefact. The best estimate of the level of activity at the time of an evoked response is one that is closest in time to it (i.e. the level of activity at which the response actually occurs). Estimating the level of activity 50 ms before stimulus onset leaves a time gap of uncertainty of 70–80 ms. The current method reduces this uncertainty to ~20 ms. The method should also be applicable to muscles with a short MEP latency, such as the biceps, as long as the recording is artefact-free and the estimation interval can be increased to improve the statistics. It should be understood that the purpose of estimating the mean background EMG in a short interval just before MEP onset was to be sure that MEP variability was not significantly due to fluctuations of the background EMG, leaving factors upstream of the motoneuron pool as the main source of MEP variability. This issue is dealt with in greater detail in the results and discussion section.

### Mathematical model

The mathematical model described here was developed to explain the sigmoid shape of MEP input–output curve, why the curve steepens when a muscle is tonically activated and why the Var–amplitude relation has an inverted parabolic shape. To this end, a minimal mathematical model that is tractable and expressed in basic neurophysiological variables was developed. Thus,  $\alpha$ -motoneurons discharge characteristics are simplified and treated as binary threshold units as follows. When the synaptic current induced by a near-synchronous corticospinal volley is sufficient to depolarize a motoneuron to threshold, a spike is discharged (Fig. 1A). The depolarization produced by a synaptic current will depend on the motoneuron’s input conductance, or equivalently its input resistance. Motoneurons of different input conductance will require synaptic currents of different strength to reach spike threshold

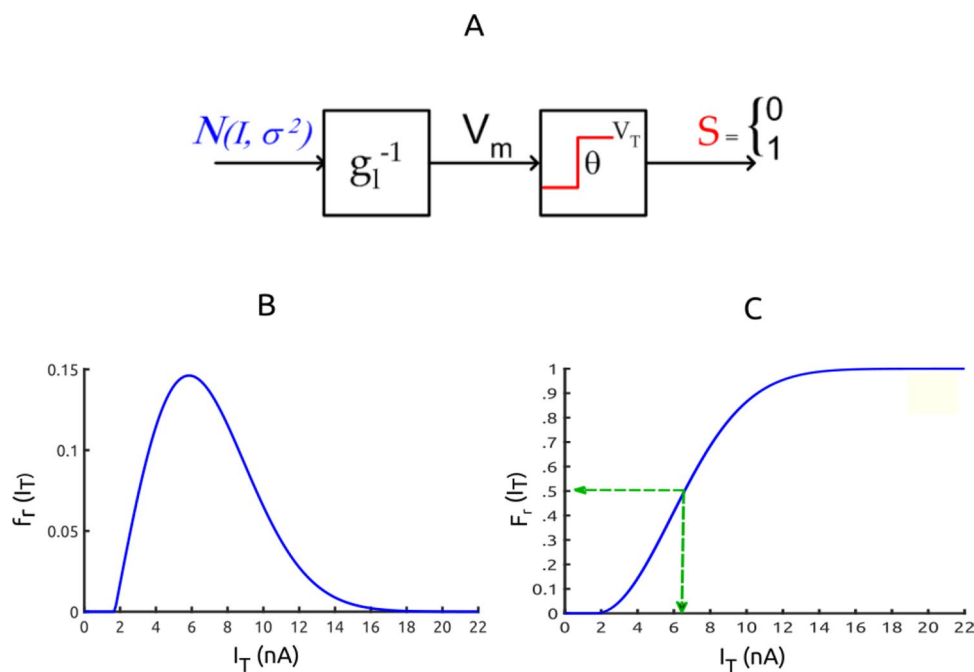


**Fig. 1** Binary threshold unit and Rayleigh probability distribution functions. **A** Shows a binary threshold unit’s characteristics in block diagram form. A noisy input current  $I$  which is  $N(I, \sigma^2)$  distributed acts through an input resistance  $g_l^{-1}$  to depolarize the membrane potential  $V_m$ . If  $V_m \geq V_T$  the unit discharges a spike,  $S = 1$ , otherwise  $S = 0$ . The Rayleigh *pdf*  $f_r(I_T)$  and *cdf*  $F_r(I_T)$  are shown in **B** and

**C**, respectively, note that the Rayleigh *pdf* is positively skewed. The parameters of the Rayleigh functions used for the numerical simulations were,  $I_{mean} = 6.9$  nA,  $I_{min} = 1.7$  nA. **C** Shows how the *cdf* determines the recruitment level of the motoneuron pool. In the example, an input current of 6.58 nA (i.e. the median value of the distribution) would recruit 50% of the units within the motoneuron pool

and thus motoneurons within a pool will be recruited in an orderly manner as a function of the input current, in accordance with the ‘size principle’. However, whilst recruitment is orderly, the recruitment rate is not uniform because a motoneuron pool is typically composed of a greater proportion of units with low input conductance (e.g.). This is accounted for by a positively skewed probability density function of input conductance (Fig. 1B, C), details of the model follow.

We will deal with the response of model motoneurons from a resting value of the membrane potential  $V_r$  to threshold  $V_T$ , where  $V_T > V_r$ . When the input current is sufficient to depolarize the membrane potential  $V_m$  to a value  $V_m \geq V_T$ , the motoneuron discharges a single spike. The response  $S$  of a binary threshold unit with input conductance  $g_l$  to an input current  $I$  is given by

$$S = H\left(\frac{I}{g_l} - \theta\right) \tag{2}$$

where  $\theta = V_T - V_r$  sets the intrinsic excitability of the unit, a post synaptic factor and  $H$  is the Heaviside step function such that

$$H(x) = \begin{cases} 1 & \text{for } x > 0 \\ 0 & \text{for } x \leq 0. \end{cases}$$

Thus, when the membrane potential  $V_m = I/g_l$  equals or exceeds  $\theta$ ,  $S = 1$  indicating spike discharge (Fig. 1A). Sub-threshold depolarization, or hyperpolarization, is effected by, respectively, changing  $V_r$  to a value closer to, or further away from  $V_T$ . The model units are not recurrently connected, consistent with the fact that motoneurons of distal muscles do not receive Renshaw cell inhibition (Windhorst 1996). As previously stated, one of the purposes of the model is to explain the nature of the Var–amplitude curve. Consequently some source of variability (i.e. ‘noise’) must be introduced in the model. Typically, when dealing with single neuron models, three sources of variability are commonly considered: variable input, variable threshold, or variable membrane potential (Trappenberg 2002). Here, we use variable input currents having a normal, or Gaussian, distribution  $N(I, \sigma^2)$  with mean value  $I$  and variance  $\sigma^2$  as shown in Fig. 1A. This choice is without loss of generality, as has been established in previous

studies (Trappenberg 2002). As will be shown, the nature of the binary threshold unit’s transfer function, Eq. 2, is markedly modified when considering noisy input currents.

The preceding paragraph describes the response of individual motoneurons to an impulse-like input current  $I$ , mimicking the near-synchronous corticospinal synaptic volley elicited by TMS. We want to determine the proportion  $R$  of motoneurons within the pool recruited as a function of  $I$ . We will refer to this proportion as the recruitment level and posit that the input–output curve is a measure of recruitment, as will be explained. The distribution of  $g_l$  within a motoneuron pool can be modelled by probability density functions (*pdf*)  $f(g_l)$  fitted to experimental data (Gustafsson and Pinter 1984). The integral of the *pdf* is the cumulative probability distribution function (*cdf*)  $F(g_l)$ , from which the proportion of motoneurons recruited by an input current can be determined (see, Capaday and Stein 1987). Figure 1C provides a graphical illustration of the procedure. Note that since the recruitment level is defined by a *cdf*, its range is  $0 \leq R \leq 1$ . The probabilistic distribution of input conductance values is a key feature of the model because, as will be shown, the nature of the  $F(g_l)$  curve contributes crucially to the shape of the input–output curve. Three different *pdfs* were used in the model simulations presented here, the uniform, exponential and Rayleigh distribution functions. These *pdfs* were chosen to contrast functions that yield sigmoid input–output curves with those that do not. Additionally, the Rayleigh *pdf* (Fig. 1B, C) fits reasonably well the distribution of input conductance of cat triceps surae motoneurons (Capaday and Stein 1987). Note that the human FDI is roughly similar in its motor unit composition (Enoka 2008). However, the distribution of FDI motoneuron thresholds is not known, whereas a reasonable estimate of this distribution is available for cat triceps surae motoneurons. The generality of the results presented here is independent of the exact distribution, or values, of motoneuron input conductance within a motoneuron pool.

The distribution of input conductance can be related to the corresponding distribution of threshold currents by  $I_T = (V_T - V_r)g_l$  - i.e. a minimum current  $I_T$  is required to discharge a unit with input conductance  $g_l$ . This directly links the input current to the proportion of units that it would recruit. In other words, the *pdfs* can be expressed in terms of the distribution of  $I_T$  rather than  $g_l$  values. The advantages of using distributions of  $I_T$  rather than  $g_l$  will be explained further on. The Rayleigh *pdf* is given by

$$f_r(I_T) = \begin{cases} \frac{2}{b}(I_T - I_{\min})e^{-\frac{(I_T - I_{\min})^2}{b}} & \text{for } I_T \geq I_{\min} \\ 0 & \text{for } I_T < I_{\min} \end{cases} \quad (3)$$

where  $I_{\min}$ , is the minimum current required to discharge the units with the lowest threshold and  $b = 4(I_{\text{mean}} - I_{\min})^2/\pi$ .

The variable  $I_{\text{mean}}$  is the mean value of current thresholds across the distribution. The uniform  $f_u(I_T)$  and exponential  $f_e(I_T)$  *pdfs* are, respectively, given by

$$f_u(I_T) = \begin{cases} \frac{1}{(I_{\max} - I_{\min})} & \text{for } I_T \geq I_{\min} \\ 0 & \text{for } I_T < I_{\min} \text{ and} \end{cases}$$

$$f_e(I_T) = \begin{cases} \frac{1}{b}e^{-\frac{(I_T - I_{\min})}{b}} & \text{for } I_T \geq I_{\min} \\ 0 & \text{for } I_T < I_{\min}. \end{cases}$$

Note that  $I_{\max}$  is the minimum current required to discharge the unit having the highest threshold and is only applicable to the uniform distribution  $f_u(I_T)$ , which is defined on the interval  $I_{\min} \leq I_T \leq I_{\max}$ . The parameter  $b$  of the exponential distribution is its mean value. For any *pdf*, the proportion  $R$  of units recruited by an input current  $I$  is given by

$$R(I_T) = \int_{I_{\min}}^I f_x(I_T)dI_T$$

where  $f_x(I_T)$  is the particular *pdf* of current thresholds. Referring to the example shown in Fig. 1C, an input current of  $I = 6.58$  nA would recruit 50% of the motoneurons in the pool.

Simulations based on the above model consist of choosing a distribution function for  $I_T$ , choosing a value for input current  $I$  and via Eq. 2 determining whether a unit is activated, or not. The proportion of units activated by that input corresponds to the recruitment level  $0 \leq R \leq 1$ . The process is repeated over a range of  $I$  values, until all the units within the motoneuron pool are recruited, i.e. when  $R = 1$ . A plot  $R$  vs.  $I$  gives the input–output, or recruitment, curve and is analogous to the experimental MEP input–output curve. If the input is noiseless, the process is purely deterministic and the recruitment variance is therefore zero. However, by randomly varying the input current  $N(I, \sigma^2)$  and repeating the simulation several times, the mean recruitment level and the recruitment variance as a function of the mean value of the input current can be numerically estimated. When motoneurons are tonically active, their membrane potential is on average closer to threshold than when they are quiescent (see, Capaday and Stein 1987). To simulate this condition,  $V_r$  is set closer to  $V_T$ .

## Results

The results section is divided in two main parts. The experimentally determined Var–amplitude and CV–amplitude relations of MEPs are first described. Subtleties of the

CV–amplitude relation are explained and examples of the amplitude distribution histograms of MEPs obtained at different stimulus intensities are described. In the second part, the mathematical model results are presented. The section begins with a description of the transfer function of binary threshold units responding to Gaussian inputs and their discharge–variance characteristics. The response properties of motoneuron pool models composed of binary threshold units are then presented. Lastly, the discharge characteristics of binary threshold units and motoneuron pool response properties are related analytically.

### Variance and CV characteristics of FDI MEPs

The input–output, Var–amplitude and CV–amplitude curves of two subjects are shown in Fig. 2. The input–output curves have the characteristic sigmoid shape that is well fitted by the Boltzmann function. The main new finding is that the Var–amplitude relation was found to have an inverted parabolic shape. The variance always peaked at an MEP amplitude near 50% of  $MEP_{max}$ , which will be referred to as  $MEP_{1/2}$ . The Boltzmann function fit to the input–output data always accounted for at least 90% of the data variance (i.e.  $R^2 \geq 0.9$ ), whereas the inverted parabola fit to the Var–amplitude data accounted for at least 86% of the data variance (i.e.  $R^2 \geq 0.86$ ), in all cases. The signal-to-noise ratio ( $snr = 1/cv$ ) is a useful measure to characterize MEP variability because the magnitudes of the variance or standard deviations are not important per se, but only in comparison to the mean. The  $snr$  calculated at  $MEP_{1/2}$ , where the variance is largest, averaged 2.96 across subjects ( $\sigma = 0.81$ ,  $range = [1.26, 5]$ ).

The CV–amplitude relation was found to have an approximately rectangular hyperbolic shape (i.e.  $CV \propto 1/MEP$ ) in most subjects (13/17). However, in a few subjects, the relation appeared to have inverse linear relation. Close inspection of the CV–amplitude relations in Fig. 2 shows that the curves appear near linear beyond MEPs of about  $1.4 \times MEP$  threshold. This strongly suggests that the inverse linear relation observed in some subjects is due to incomplete sampling of the input–output curve, or a discontinuity of MEP amplitude, near the foot of the curve in each case. Evidence of this can be seen in the input–output curves shown in Fig. 3. In the example shown in Fig. 3A, there is a jump in MEP amplitude near the foot of the input–output curve and in Fig. 3B, the curve is not sampled at the foot of the curve.

### MEP amplitude distribution histograms

Figure 4 shows examples of MEP amplitude distribution histograms at two stimulus intensities. The distribution of MEP amplitudes appears random and is not obviously similar to standard *pdfs*, such as the Gaussian, uniform,

or exponential. However, note that at low-stimulus intensities, the distribution is relatively narrow and skewed to the left, that is, toward low amplitude MEPs. At intermediate-stimulus intensities, the mean value of the distribution increases and the histogram broadens. Put another way, the variance was small at low-stimulus intensities and larger at intermediate-stimulus intensities for all subjects, as expected from the Var–amplitude relations in Fig. 2. These results are in keeping with those reported by Goetz et al. (2014), despite the far lower number of MEPs used to construct their amplitude histograms. Importantly, MEP amplitude variability was not related to fluctuations in the background EMG. For example, for the data presented in Fig. 4B, the fluctuations of background EMG account for only 3.2% of the MEP variance (i.e.  $r^2 = 0.032$ ,  $p = 0.04$ ). In no case did fluctuations of the background EMG account substantially for MEP variance. This strongly suggests that the MEP fluctuations were not due to fluctuations of the background EMG, but to factors up-stream of the motoneuron pool. Of note, there was no correlation between the mean value of the background EMG measured during 50 ms before stimulus onset with that measured during 20 ms before MEP onset ( $r^2 = 0.017$ ,  $p = 0.14$ ). More importantly, the mean EMG measures over the 50 ms interval before stimulus onset were not correlated with FDI MEP amplitude in all five subjects ( $r^2 = 0.003$ ,  $p = 0.53$ ).

The experimental observations reported in the preceding paragraphs are explained by the first-order mathematical model described in the methods section, as follows.

### Input–output characteristics of binary threshold units

The response characteristics of a binary threshold unit are shown in Fig. 5. Clearly, when the input current is constant, the transfer function is step-shaped (Fig. 5A) as described by Eq. 2. The unit does not discharge unless the input  $I \geq I_T$  and there is no discharge variability, it will always fire when this condition is met. By contrast, when the input current is noisy with Gaussian statistics  $N(I, \sigma^2)$ , the transfer function is sigmoid-shaped (Fig. 5A), meaning the unit now responds only on a proportion of trials. The discharge variance plotted against the discharge probability follows a parabolic profile (Fig. 5B), reaching a peak of 0.25 when the discharge probability  $p = 0.5$ , regardless of the variance of the input. The sigmoid shape of the transfer function and the parabolic shape of the discharge variability are explained as follows.

The discharge probability curve in Fig. 5A gives the proportion of trials for which the noisy input current  $I \geq I_T$ . For example, at a mean value of  $I = I_T$ , the response probability is  $p = 0.5$ , because Gaussian noise has on average 50% of values above and below the mean. For inputs whose mean value is below threshold, there is a

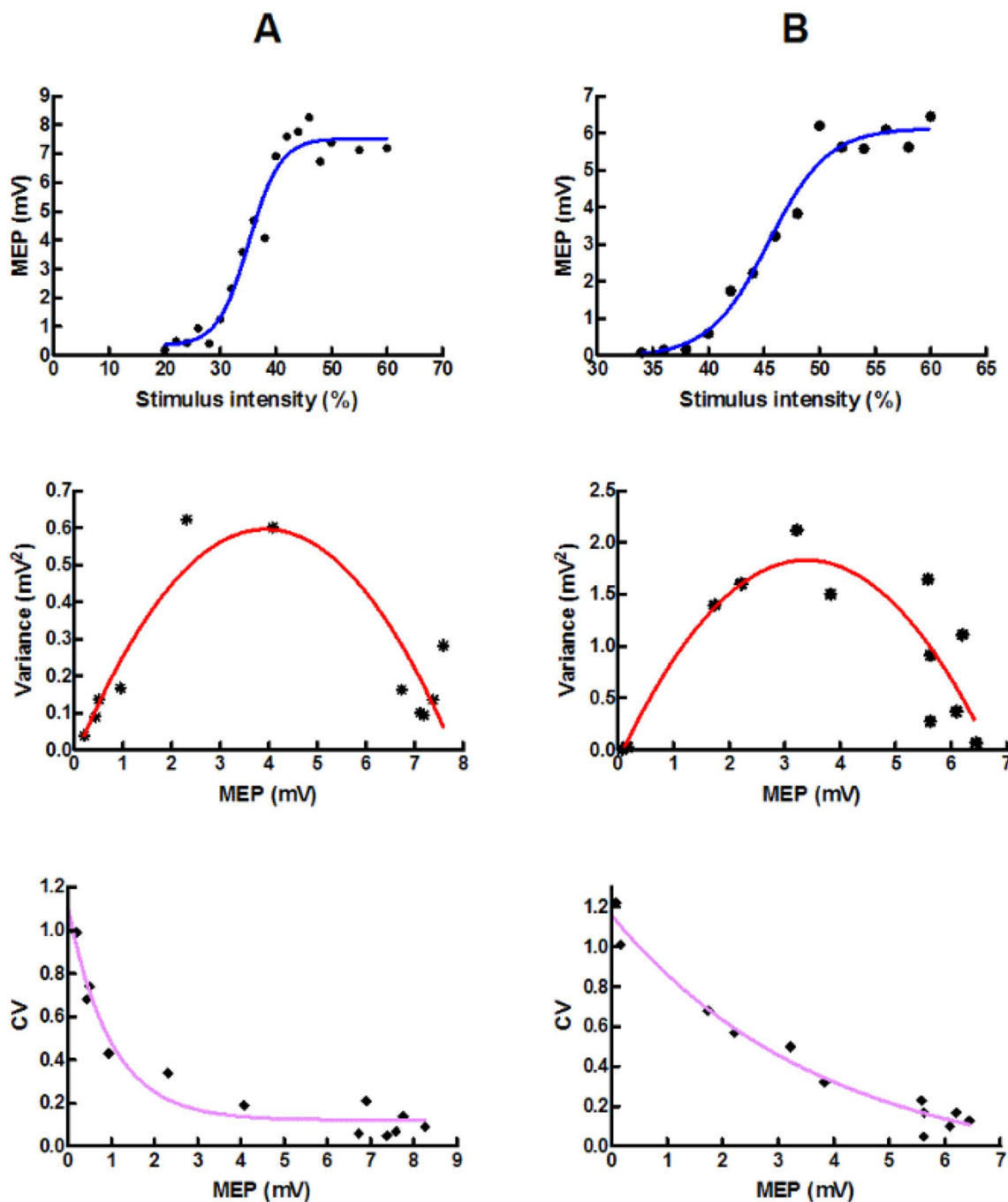


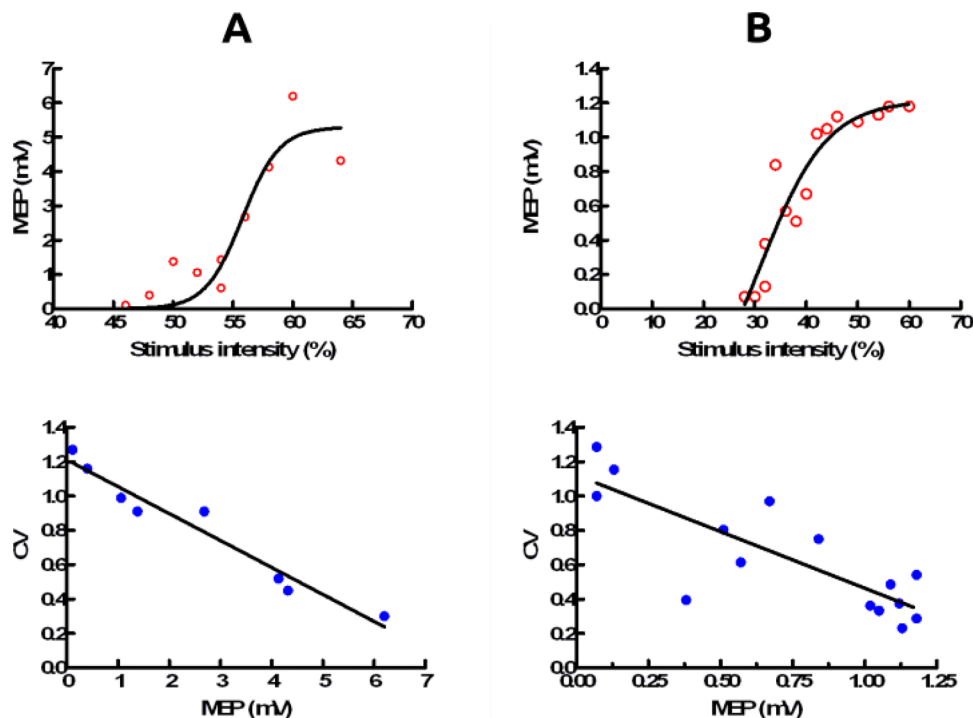
**Fig. 2** Examples of input–output, Var–amplitude and CV–amplitude curves. Panels **A**, **B** are data from two different subjects. Note the sigmoid shape of the input–output curves, the parabolic shape of the Var–amplitude curves and the hyperbolic shape of the CV–amplitude

curves. In all cases shown, the goodness of fit value was  $R^2 \geq 0.95$ . Note that some of the points in the Variance vs. MEP plot in (**A**) fall on top of each other; hence, the graph may appear to have fewer points than its counterparts above and below

proportion of trials for which  $I \geq I_T$ . Noise will thus make the unit fire for mean values below  $I_T$ . The less than unity probability of discharge (i.e.  $p < 1$ ) for inputs whose mean is above threshold is explained in a similar manner, there is a proportion of trials for which  $I < I_T$ . As  $\sigma^2$  increases, the foot of the transfer moves to the left along the abscissa and

the steepness of the curve decreases (Fig. 5C). Increasing  $\sigma^2$  broadens the width of the distribution and lengthens the tails. It can thus be inferred that there will be a greater proportion of small mean input values that exceed  $I_T$  and a larger proportion of high mean input values that do not. Consequently, the transfer function will rise more slowly

**Fig. 3** Examples of linear-like CV–amplitude relations obtained in two subjects In A, there is a jump in MEP amplitude near the foot of the of the input–output curve at a stimulus intensity of ~50% and in Fig. 3B, the foot of the curve is incompletely sampled



and its foot will shift to the left. The smaller the variance of the input, the closer the transfer function is to the step-change transfer function for noiseless inputs.

From the above considerations, it follows that the transfer function of the binary threshold unit driven by Gaussian noise is

$$p(S = 1) = \frac{1}{2} \operatorname{erfc} \left( \frac{I_T - I}{\sigma \sqrt{2}} \right), \quad (4)$$

where  $\operatorname{erfc}$  is the complementary error function and  $\sigma$  the standard deviation of the noisy input current  $I$ . The equation gives the probability of spike discharge. The notation  $p(S = 1)$  refers to the probability that the spiking variable in Eq. 2 has a value of  $S = 1$ . For example, when  $I = I_T$ ,  $p(S = 1) = 0.5$ . The slope of the transfer function at the half-maximal input value  $I_T$  is  $1/\sigma\sqrt{2\pi}$ , decreasing with increasing noise level, as explained above. A plot of Eq. 4 for a unit with an  $I_T$  value of 10 nA and  $\sigma^2 = 3$  is shown in Fig. 5A, the equation fits very closely the numerical simulations. For a given value of  $\sigma$ , subthreshold depolarization leads to a leftward shift of the input–output curve along the abscissa, which is readily verifiable by substituting  $I_T$  with  $g_I\theta$  in Eq. 4.

The parabolic shape of the discharge variance curve (Fig. 5B) is explained as follows. Activation of a unit by a noisy current  $N(I, \sigma^2)$  repeated several times in succession is equivalent to series of Bernoulli trials, with probability  $p$  of firing and probability  $q = (1 - p)$  of not firing in response to a noisy input current  $N(I, \sigma^2)$ . The variance of Bernoulli

trials depends only on the probabilities of success  $p$  and failure  $q$  and is given by  $\operatorname{var}(p) = p(1 - p)$ . The graph of the equation is clearly an inverted parabola that fits very closely the results of the simulation runs as shown in Fig. 5B. The neurophysiological interpretation of the variance equation is akin to that for coin tossing experiments. The variance is maximal when the probability of success, or failure, is  $p = q = 0.5$ . When the probability of success is  $p = 1$ , the discharge variance is zero, since the unit always fires. When  $p = 0$ , the unit never fires; hence, the discharge variance is also zero. Related to the variance, the CV of Bernoulli trials is given by  $\operatorname{CV} = \sqrt{(1 - p)/p}$ , this fits quite well the numerical simulations results shown in Fig. 5D.

### Input–output characteristics of motoneuron pool models

In this section, we deal with the recruitment of binary threshold units within a pool. The distribution of the input conductance  $g_i$  of the units within the pool is described by one of the three *pdfs* listed above. Figure 6A shows the recruitment level as a function of a noise-free input current for each *pdf*. There are two noteworthy points to consider: first, the recruitment in each case follows, by definition, the shape of the respective *cdf*, second, the recruitment curve is a sigmoid only for the Rayleigh *pdf*. The exponential and uniform *pdfs* do not produce a sigmoid-shaped recruitment curve, contrary to what is observed experimentally for MEPs and MSRs. Activation of the units with noisy input currents

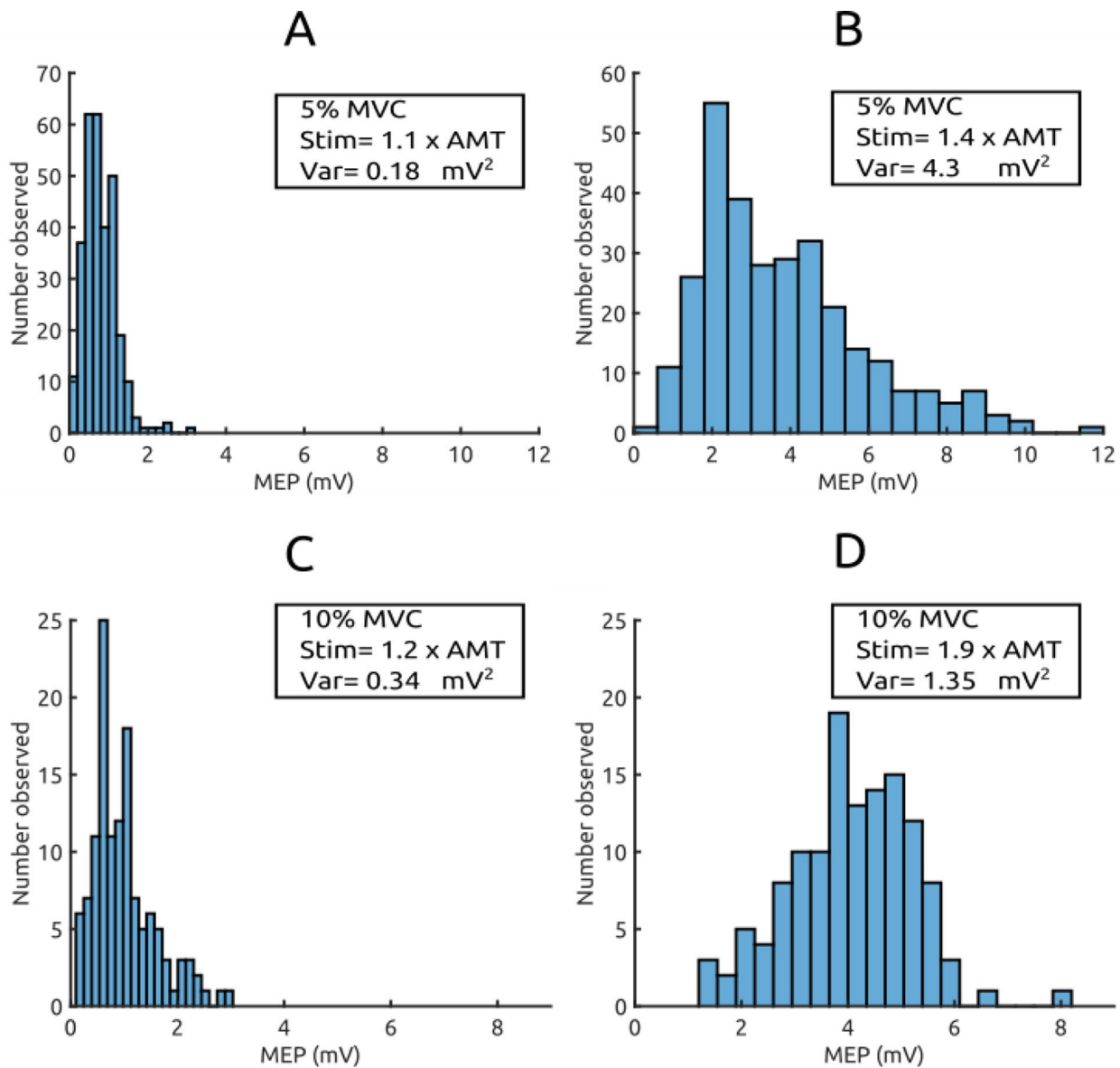


**Fig. 4** MEP amplitude histograms of two different subjects for low and intermediate intensity stimuli. Note that at low-stimulus intensity (A and C), the histograms are positively skewed and have relatively

low variance. For stronger stimuli (B and D), the histograms broaden, hence the variance increases. In no case does the histogram resemble any common *pdf*, such as a Gaussian, exponential or uniform

does not change the basic shape of the recruitment curve (Fig. 6B–D). However, in all cases, the recruitment curves are modified by noisy inputs in three principal ways. As can be observed in the figures, the foot of the response is shifted to the left along the abscissa (i.e. decrease of threshold), the recruitment rate (i.e. slope of the curves) decreases and maximum recruitment is never quite reached. The decrease of the recruitment rate is less pronounced for the uniform distribution (Fig. 6D).

For the remainder of this section, we will deal with recruitment in a motoneuron pool having a Rayleigh distribution of  $g_l$  driven by noisy input currents  $N(I, \sigma^2)$ . The

recruitment level  $R$  and variance–recruitment  $\text{Var}_R - R$  curves are shown in Fig. 7A, B. The  $R$  curve is sigmoid-shaped and the  $\text{Var}_R - R$  curve is an inverted parabola, consistent with the experimental observations presented. It is important not to confuse the  $\text{Var}_R - R$  curve—a population variable—with the discharge variance curve of single units. The maximum value of  $\text{Var}_R$  occurs when the recruitment level is very nearly 50% (i.e. at  $R_{1/2}$ ), again consistent with the experimental results. Note however, that the  $\text{Var}_R - R$  curve is slightly asymmetric, rising more steeply for inputs less than  $I = 6.58nA$  and more slowly for input  $I > 6.58nA$ . This is because the Rayleigh *pdf* is

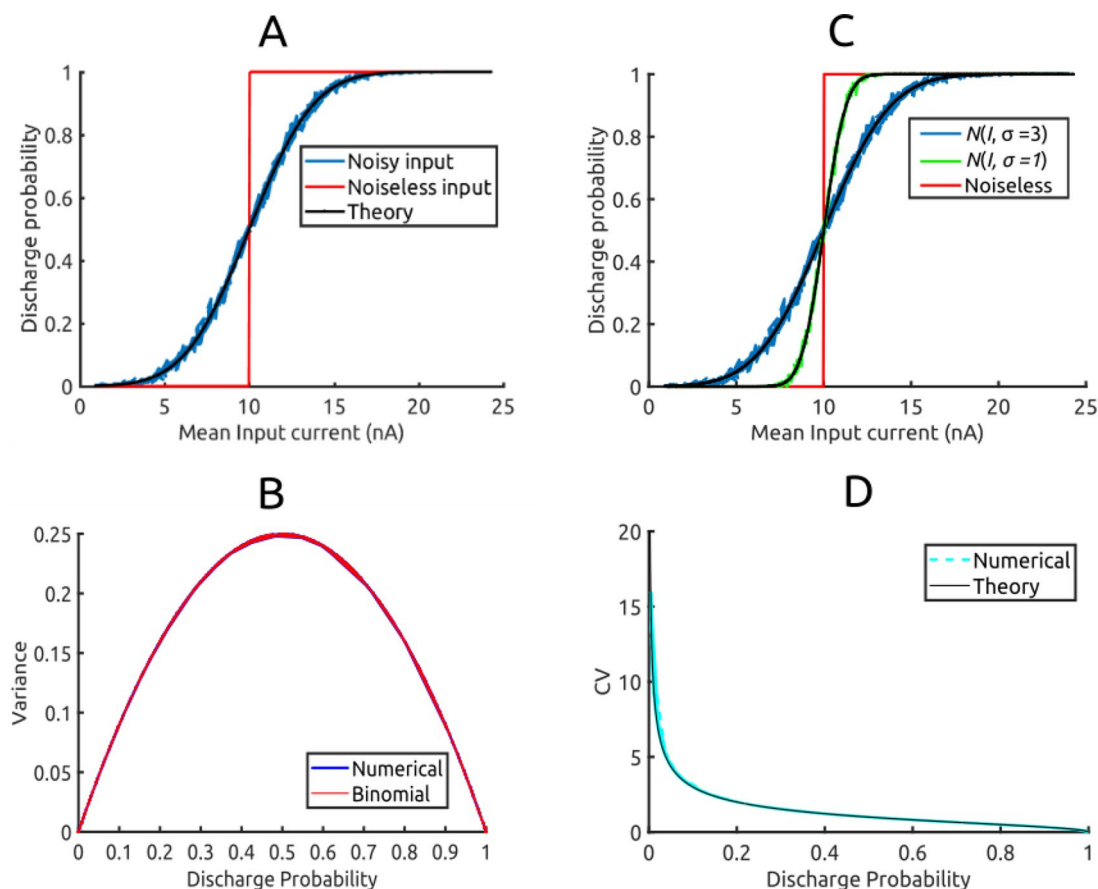


**Fig. 5** Response characteristics of binary threshold units. **(A)** The response of a binary threshold unit with an  $I_T$  value of 10 nA to noise-free input currents, or to noisy inputs having a normal distribution  $N(I, \sigma^2)$ . Note that the transfer function for the noise-free inputs is the Heaviside step function, shown in red. The solid black curve (Theory) going through the points of the numerical simulation runs ( $n=256$ ) is the discharge probability predicted by Eq. 4. **(B)** When the

positively skewed (Fig. 1B), with  $I = 6.58$  nA being the median value of the distribution. Thus, half the units have an  $I_T$  value between 1.7 nA and 6.58 nA, a range of 4.88 nA, whereas the other half have an  $I_T$  value between 6.58 nA and  $\sim 20$  nA, a range of 13.42 nA. Sub-threshold depolarization (i.e. reducing the voltage threshold  $\theta$ ) results in a steeper recruitment curve (Fig. 7A). This is akin to the steepening of the MEP input–output curve when a subject exerts a tonic background contraction compared to rest (Devanne et al. 1997). Additionally, the  $\text{Var}_R - R$  curves are scaled up by a multiplicative factor (Fig. 7B). In other words, the variance increases independently of the recruitment level over nearly all the recruitment range. This is due to the compression and up-scaling of the distribution of  $I_T$  (Fig. 7D). The  $\text{CV} - R$  curve decreases along an approximately rectangular hyperbolic profile (Fig. 7C), similarly to the experimental  $\text{CV}$ –amplitude curves. Interestingly, increasing the noise level, or decreasing  $\theta$  results

unit responds to noisy inputs, the discharge variance vs. the response probability has an inverted parabolic profile, as predicted by the Bernoulli probability model. Note that when the noisy input current  $I$  is equal to  $I_T$ , the discharge probability is  $p = 0.5$  and the discharge variance is maximal. **(C)** Increasing the noise level decreases the slope of the transfer function and lowers the threshold. **(D)** The CV decreases as  $\sqrt{(1-p)/p}$ , as predicted by the Bernoulli probability model

in a nearly linear  $\text{CV} - R$  curve, reminiscent of the experimental results shown in Fig. 3.

### Relation between input–output and recruitment curves

The size of motor unit action potentials (MUAP) increases with recruitment order. However, the relation between input conductance  $g_I$  and MUAP size is not known. Fuglevand et al. (1993) suggested that MUAP size grows exponentially with recruitment order, over a 100-fold range. The nearly synchronous activation of motor units produced by a single TMS stimulus results in a compound action potential (CAP), termed MEP. The CAP is the result of algebraic summation of individual MUAPs. How would scaling the recruitment curve  $R(I)$  in terms of CAP size affect its shape? To answer this question, the  $R(I)$  curve and its scaled CAP version are shown in Fig. 8A. The CAP is composed of MUAPs whose

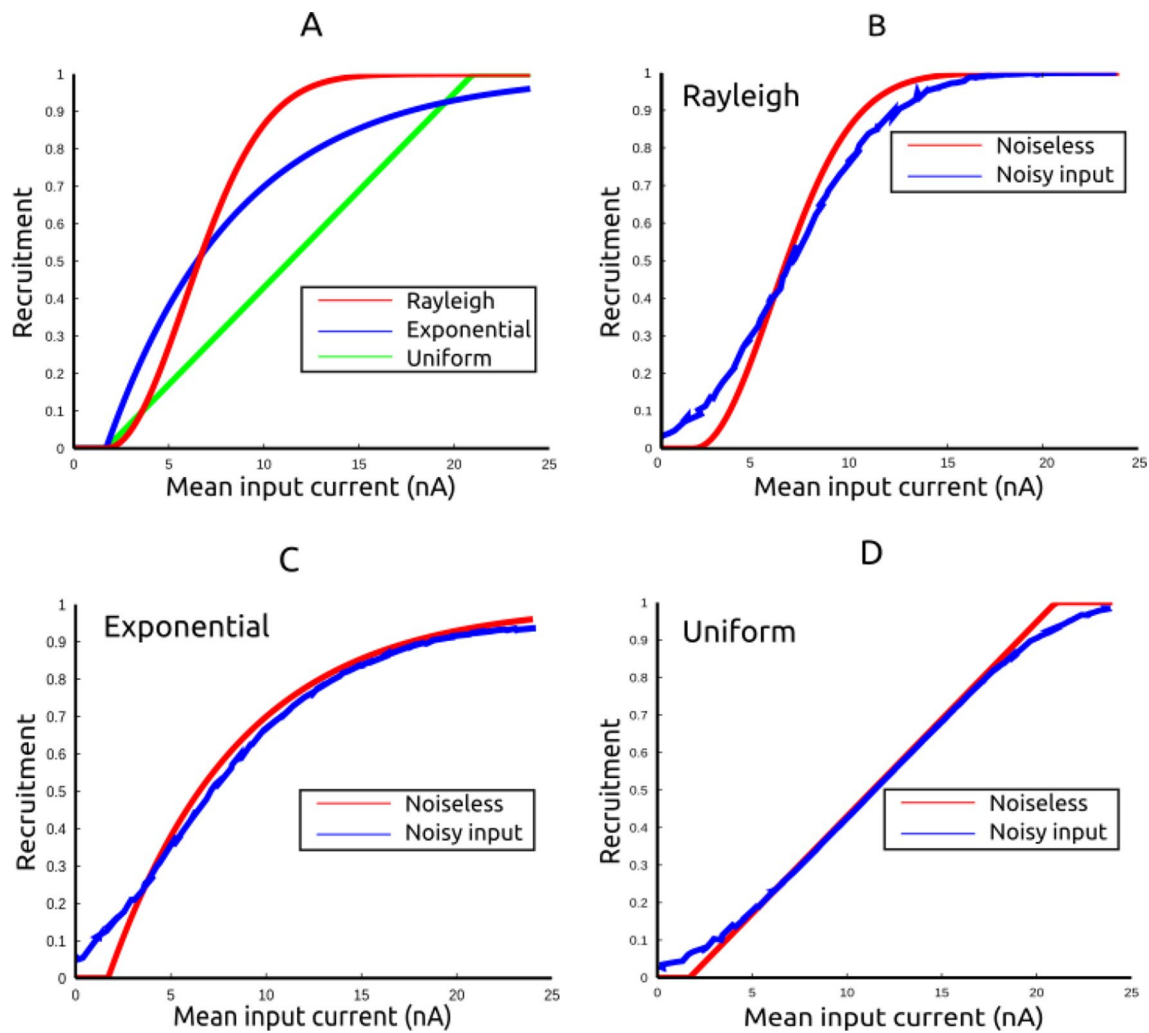


**Fig. 6** Contrasting the shapes of input–output curves. The form of the input–output curves for the Rayleigh, exponential and uniform pdfs are show in A. Note that only the Rayleigh pdf results in a sig-

moid-shaped input–output curve. In all cases, noisy input currents decreased the slope and reduced the threshold of the input–output curve

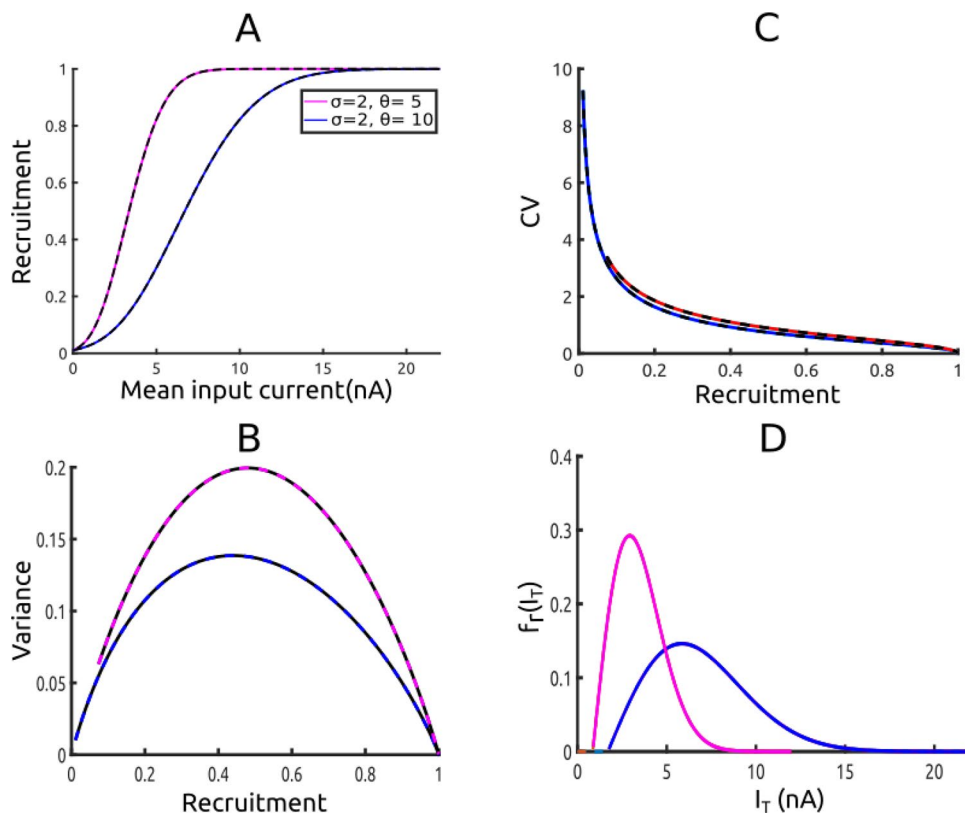
size grows exponentially with recruitment order, over a 100-fold range. As can be seen, both curves are a sigmoid function of the mean input current and the CAP is proportional to  $R$ , albeit nonlinearly (Fig. 8B). One can also suggest, for example, that MUAP size grows linearly with recruitment order. Surprisingly, even in this case, the CAP curve remains a sigmoid and the two curves are not linearly related. The sigmoid nature of the recruitment curve leaves its imprint. Only if the MUAP size is distributed in the same way as  $g_l$ , which determines the recruitment order, would the two curves be sigmoids and linearly proportional to each other.

**Recruitment distribution histograms**

The recruitment distribution for low, intermediate and high mean input currents is shown in Fig. 9. In all cases, the variance of the noisy input current is  $\sim 4.0 \text{ nA}^2$ , and their

distribution is essentially Gaussian as can be seen in the lower panels of the figure. By contrast, observe that the recruitment distribution histograms are not Gaussian and that the shape of the distribution changes as a function of the mean input current. For low mean input currents, the recruitment distribution histogram is positively skewed towards low recruitment values and for strong mean input currents, it is negatively skewed towards high recruitment values (Fig. 9A and C). Note that in each case, the distribution is narrow, reflecting low variance. For intermediate-strength inputs near the half-maximum input current  $I_{1/2}$ , the distribution is much broader, reflecting high variance (Fig. 9B). These modelling results reflect the experimental findings shown in Fig. 4, at low and high recruitment levels, the variance is small, whereas near  $I_{1/2}$  the variance is maximal.

**Fig. 7** Main results of the numerical simulation of the motoneuron pool model. The simulation used noisy input currents with  $\sigma = 2nA$ , repeated 512 times. **A** The recruitment curve has a sigmoid shape which steepens if the threshold  $\theta$  of the binary-units is reduced ( $\theta = 10$  vs  $\theta = 5$ ). The recruitment–variance curve is parabolic and the curve is scaled up by a multiplicative factor when the threshold is reduced **B** and the CV vs. recruitment curve resembles a rectangular hyperbola (**C**). A reduction of  $\theta$  compresses and scales up the distribution of  $I_T$  (**D**). Solutions of the model summary Eqs. 5 and 7 are plotted with the numerical simulation results as black dashed marks. The reader should note the similarities between the model results and the experimental results presented in Figs. 2 and 3



**Relating binary threshold unit responses to motoneuron pool response**

Consider binning the Rayleigh pdf in Fig. 1B into  $N$  bins of width  $2\Delta I_T$ . The area of each bin gives the proportion  $b_i$  of units within the bin interval  $I_{T_i} - \Delta I_T \leq I_T \leq I_{T_i} + \Delta I_T$ , where  $1 \leq i \leq N$  refers to the bin number. If the bins are small enough, the discharge probability  $p_i$  of the units within a bin is approximately equal to that of the unit with an  $I_{T_i}$  value in the middle of the bin. Since  $p_i$  is a function of the input current given by Eq. 4, we can write  $p_i(I)$ . Considering the  $i$ th bin, the average or expected proportion of units  $r_i$  that would be recruited by an input current  $I$  would be  $r_i(I) = b_i p_i(I)$ . The population response  $R(I)$  is the sum over all bins, thus

$$R(I) = \sum_{i=1}^N b_i p_i(I). \tag{5}$$

In the continuous case, the summation operator would be replaced by an integral of the discharge probability Eq. 4 multiplied by the Rayleigh pdf. Keep in mind that  $R(I)$  is the expected or mean recruitment level and therefore a probabilistic variable.

For the recruitment variance, recall that a single unit’s discharge variance is  $p(I)(1 - p(I))$ , therefore the recruitment variance within a given bin is  $b_i p_i(I)(1 - p_i(I))$ . Since

the units and bins are independent, the population variance is the sum of the individual variances. Following algebraic manipulations, it can be shown that the recruitment variance of the population  $\text{Var}_R(I)$  is given by

$$\text{Var}_R(I) = R(I) - \sum_{i=1}^N b_i p_i(I)^2 \tag{6}$$

Furthermore, the recruitment variance can be expressed in terms of the recruitment level by substituting  $p_i(I) = r_i(I)/b_i$  in the preceding equation, obtaining

$$\text{Var}_R(I) = R(I) - \sum_{i=1}^N \frac{r_i(I)^2}{b_i}. \tag{7}$$

The limiting values are  $\text{Var}_R(R = 0) = 0$  and  $\text{Var}_R(R = 1) = 0$ , as expected. Moreover, because the function is quadratic, there is only one maximum between the limiting values. This maximum occurs at  $R(I) = \sum_i \frac{b_i}{2} = 0.5$ , the median value of the distribution. Since the Rayleigh pdf is positively skewed (i.e. its median value is less than its mean value), the  $\text{Var}_r - R$  curve can be slightly asymmetric depending on the noise level or firing threshold (Fig. 6B). The preceding three equations are a succinct summary of the model presented, relating single-unit transfer functions to motoneuron pool response characteristics. They accurately fit the numerical simulation results as shown in Fig. 7.

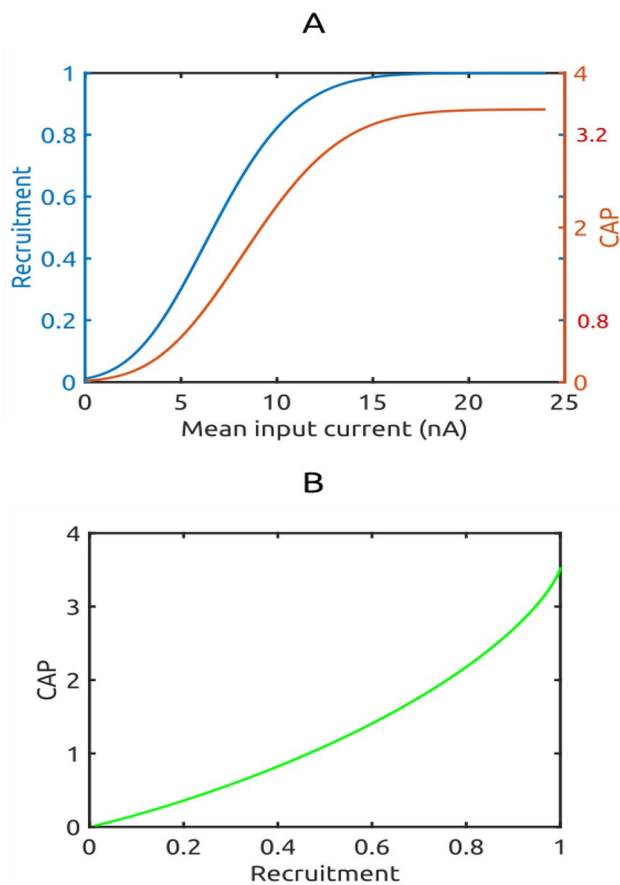


**Fig. 8** Relation between input–output and recruitment curves. The double y-axis graph in **A** shows the recruitment curve and its scaled CAP version as a function of the mean input current. The CAP curve is computationally equivalent to an experimental MEP input–output curve, but its scaling is arbitrary. Note that the two curves whilst proportional to each other, are not linearly related (**B**)

### Discussion

The main new experimental finding reported herein is that the relation between MEP variance and amplitude is an inverted parabola that peaks at  $\sim \text{MEP}_{1/2}$ , or equivalently at  $S_{50}$ . It was also shown that CV–amplitude relation resembles a rectangular hyperbola and explained why in some cases an inverse linear relation is obtained. It is due to incomplete sampling of the MEP input–output curve near the foot of the relation, or more rarely because of a response discontinuity near threshold. Note that the CV–amplitude relation was described as approximately hyperbolic because of the square root dependence of the single-unit CV (i.e.  $CV = \sqrt{(1 - p/p)}$ ). The CV will thus decrease more slowly as a function of MEP amplitude in comparison to a hyperbolic relation. Data were also presented on the amplitude distribution histograms of MEPs for low- and intermediate-strength stimuli. At low-stimulus intensities, the histograms are narrow and positively skewed with small mean value and variance. They broaden at intermediate-stimulus intensities with a larger mean and variance. Their form thus changes with stimulus intensity. The histograms do not resemble any obvious theoretical probability distribution functions, such as the Gaussian, Rayleigh, or uniform distribution. The first-order probabilistic model developed in the methods section explains well the experimental results, including the shape of the input–output curve, as follows.

The sigmoid shape of the MEP input–output curves arises from the shape of the *cdf* describing the distribution of input conductance  $g_I$ , or equivalently threshold currents  $I_T$ . As the input current increases, recruitment proceeds along the curve described by the *cdf* (Fig. 1C). Noisy input currents decrease the steepness of the curve and lower the threshold for the following reasons. Because the input is noisy, there is some chance that low values of the input current exceed the  $I_T$  of low threshold units, recruitment

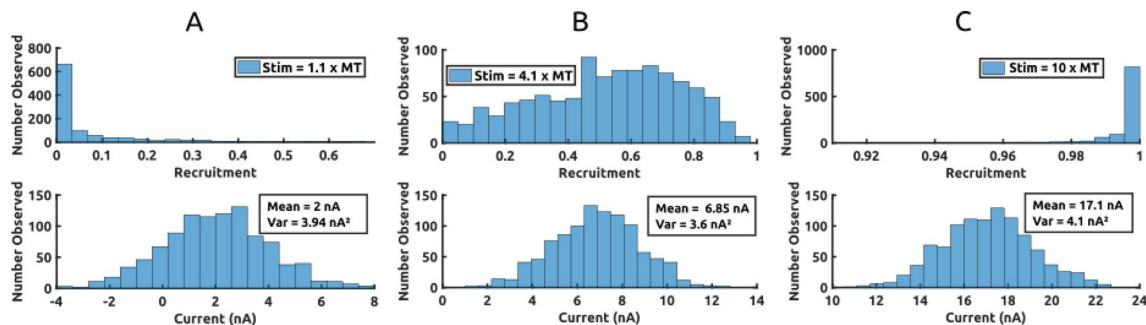


**Fig. 9** The recruitment distribution histograms (upper panels) are not Gaussian. Note how the shape of the distribution changes as a function of the mean input current. By contrast, note the Gaussian nature of the input current amplitude histograms in the lower panels. The

upper panels display stimulus strength in terms of the ‘motor threshold’ (MT) for comparison to experimental data, whereas the lower panels display the actual value of the input current and its variance

is thus increased at the low end. At the high end of the *cdf* (i.e.  $I_T > I_{1/2}$ ), the input is below the threshold of these units half the time, recruitment is thus decreased. Taking these two points together leads to a slower recruitment rate. By contrast, decreasing the unit thresholds (i.e. increased background synaptic drive) increases the steepness of the curve, whether the inputs are noisy or not. This gain change is simply explained by the fact that motoneurons are recruited at a faster rate when their effective threshold is lowered. It can also be understood by considering that a decrease of threshold compresses and scales up the *pdf* curve (Fig. 7D), consequently full-scale recruitment occurs over a narrower range of input currents. Importantly and contrary to what has been reported for previous models (Capaday 1997; Rall 1955b), the input–output curves do not shift in parallel along the input axis with changes in motoneuron excitability. This is only true for the transfer function of binary threshold units, the gain change is thus a population effect. Not all *cdfs* have a sigmoid shape and not all that do, like the Gaussian, fit the positively skewed distribution of motoneuron pool threshold currents. A positively skewed distribution with a sigmoid *cdf*, like the Rayleigh distribution, is required. The exponential *pdf* has often been used to describe the distribution of motoneuron threshold current values (e.g. see, Fuglevand et al. 1993; Keenan et al. 2006). However, this *pdf* does not have sigmoid-shaped *cdf* and thus cannot be the basis of a sigmoid input–output curve. Additionally, the exponential *pdf* is not physiologically realistic since it has a discontinuity at the threshold current  $I_{\min}$ .

The inverted parabolic shape of the  $\text{Var}_R - R$  relation and by analogy that of the experimental Var–amplitude relation are explained as follows. Near  $R_{1/2}$ , or equivalently  $I_{1/2}$ , the median value, low and high  $I_T$  units contribute little or nothing to the recruitment variance. Low threshold units at input current values near  $I_{1/2}$  are saturated, so their  $\text{var} \approx 0$ . High  $I_T$  units are for the most not discharged, so their  $\text{var} \approx 0$ , or very low. Whilst near  $I_{1/2}$  you have the highest density of units (Fig. 1B) and since their  $I_T$  is near  $I_{1/2}$ , their discharge  $\text{var}$  is high (Fig. 4B). Recall that  $\text{Var}_R$  is the sum of the individual variance  $b_i p_i (1 - p_i)$ . Clearly, it will follow a parabolic curve, peaking at  $I_{1/2}$  when  $p = 0.5$  and the density  $b_i$  is highest. By contrast, the  $\text{Var}_R - R$  relation for a uniform distribution of  $I_T$  is constant over most of the recruitment range  $\sim 0.2 \leq R \leq 0.8$ , because the density of all bins is equal. As noted in the results section, the degree of asymmetry of  $\text{Var}_R - R$  curve is dependent on the noise level of the input currents and the threshold, being negligible for values of  $\sigma > 2$ , or  $\theta < 7$ . Interestingly, the Var–amplitude of MSRs recorded from the S1 ventral root, which contains a large proportion of the soleus motoneuron axons, is asymmetric (Rudomin 1980; Rudomin and Dutton 1969). This is expected given low-noise synaptic inputs and a strongly

positively skewed distribution of feline soleus motoneuron input conductance values.

Relatedly, the Var–amplitude characteristics of MEPs in different muscles may be expected to show asymmetries consistent with their MU compositions, considering the details just discussed. It would thus be interesting to measure Var–amplitude characteristics of different muscles, such as biceps, whose recruitment range is broader than that of the FDI—i.e.  $\sim 90\%$  of MVC vs.  $\sim 60\%$  MVC (e.g. see Dideriksen et al. 2012). It may turn out that the Var–amplitude asymmetry reflects differences in recruitment range between different motoneuron pools. The model predicts that strongly positively skewed distributions of input conductance will result in a Var–amplitude relation with a peak that is shifted to the left (i.e. to lower recruitment levels), whereas a strongly negatively skewed distribution will produce a Var–amplitude relation that is shifted to the right. It may thus be possible to infer the nature of the input conductance distribution of different motoneuron pools.

The model predicts that MEP variance should increase with the level of  $\alpha$ -motoneuron drive (voluntary EMG activity), independently of MEP amplitude (Fig. 7B). This can be understood by the compression and multiplicative scaling of the *pdf* produced by depolarization, as shown in Fig. 7D. Recall that the *pdf* gives the density of units per unit  $I_T$ . Thus, compression and scaling of the *pdf* imply that within any bin  $b_i$  of width  $\Delta I_T$ , the proportion of units will be greater and consequently the variance  $b_i p_i (1 - p_i)$  will be greater for any value of  $p_i$ . Darling et al. (2006) reported that an increase of  $\alpha$ -motoneuron drive, relative to rest, results in an increase of MEP variance when plotted vs. stimulus intensity. This would also be true if the variances were plotted vs. MEP amplitude and is therefore as predicted by the model. However, it was also reported that the CV plotted vs. stimulus intensity decreased, which seems surprising and contrary to the model results which show that CV should slightly increase (Fig. 7C). This apparent discrepancy is explained as follows. Increasing  $\alpha$ -motoneuron drive steepens the input–output curve, which means that MEPs increase at a faster rate as a function of stimulus intensity, but the variance increases more slowly. Consequently CV appears lower when plotted against stimulus, but higher when plotted vs. MEP amplitude. In short, the model's prediction on MEP variance is fully consistent with and clarifies the available experimental evidence.

Regarding the MEP amplitude histograms, one may surmise that for any stimulus intensity, the distribution should reflect the noise characteristics of the evoked corticospinal synaptic currents, say for example Gaussian. However, whatever the statistical characteristics of the synaptic currents may be, one also needs to consider that these act on a non-homogenous population of motoneurons having a positively skewed distribution of input conductance. Consequently, the

distribution of MEP amplitudes will depend on the *pdf* of the synaptic current amplitudes, as well as the distribution of input conductance. The resulting amplitude histograms will resemble neither distribution and their shape will change with stimulus intensity. The model thus explains the nature of the observed experimental MEP amplitude histograms.

The Boltzmann equation, which has been widely used to fit MEP input–output curves, is not derived from the model presented. *viz.* binary-variable-threshold units driven by noisy synaptic currents, with unit threshold currents distributed according to a positively skewed probability density function. The Boltzmann model derives the actual distribution of, for example, the number of molecules at different energy levels. It predicts an exponential decrease of the number of molecules with increasing energy level. Similarly, Hodgkin and Huxley characterized the voltage dependence of ionic membrane conductance based on a Boltzmann distribution of the proportion of charged molecules on the inside of the membrane relative to the outside (Hodgkin and Huxley 1952). The present model does not predict an exponential decrease of the number of recruited units with increasing  $I_T$ . What then is the connection between the present model and the Boltzmann equation? One may surmise that the distribution of input conductance within motoneuron pools, such as that of the FDI, is a Boltzmann-like function. However, whilst the Boltzmann *cdf* has a sigmoid shape, the *pdf* is a symmetrical bell-shaped curve, which would imply that the distribution of motoneuron input conductance is symmetric. This is counter to the available evidence, as previously discussed. Nonetheless, the defining equation of the Boltzmann *cdf* has sufficient parameters ( $S_{50}$  and slope parameter) to obtain a good fit with experimental data. In the absence of direct measurements of the distribution of input conductance, or relative excitabilities of motoneurons within a pool, the Boltzmann function remains a useful empirical fit to MEP input–output curves and several statistical methods have been proposed to determine task-dependent changes of these curves (e.g. Devanne et al. 2002; Kouchtir-Devanne et al. 2012).

As the experimental results show and the model explains, MEP amplitudes are not normally distributed and their variance is not homogeneous. Additionally, as shown in Fig. 7D, MEPs obtained in different conditions are drawn from distributions having different mean and variance. These results have implications for statistical analysis, a conclusion also reached by Goetz et al. (2014). Unpaired t tests, ANOVA and curve-fitting algorithms, for example, assume that the variables are at least roughly normally distributed with equal variance (e.g. see Devore 1987). While Monte Carlo simulations have shown that these tests are relatively robust to departures from these assumptions (e.g. see Ferguson 1976), it remains to be determined whether this is also true for MEPs given the statistical characteristics reported here. For example, it

would be of interest to determine whether weighted non-linear curve-fitting algorithms yield more robust results than standard non-weighted algorithms. Importantly, the type of weighting (e.g.  $1/x$ ,  $1/x^2$  etc.) needed to improve the quality of fit depends on knowledge of the functional relation between MEP amplitude and variance (e.g. see Devore 1987).

At constant stimulus intensity, there are two sources of MEP variability, variability of corticospinal synaptic transmission and variability due to motoneuron membrane potential fluctuations, both are inherent to the present model. Many studies have been done to find experimental protocols that minimize MEP variability and reliability of input–output curves (Julkunen et al. 2012; Pellicciari et al. 2016; Suckley et al. 2020; Keirs et al. 1993). It is suggested that by far the most influential and controllable variable is the background level of EMG activity, a measure of motoneuron pool recruitment level and firing rate ( $\alpha$ -motoneuron drive). Indeed, the recent study of Suckley et al. (2020) with background contraction of the FDI maintained at 10% of MVC, no statistically significant differences in MEP variance between three blocked stimulation protocols were found. MEP amplitude is highly sensitive to changes in the background EMG level, at a fixed stimulus strength, MEPs increase linearly with the mean level of background EMG (e.g. Darling et al. 2006; Lavoie et al. 1995). Importantly, it is the EMG level just prior to MEP onset that is important and not, as is usually done, that measured 50–100 ms before the stimulus. In other words, it is the near instantaneous level of background EMG and the co-temporal noisy synaptic input, which determine MEP amplitude. Such a near instantaneous measure of EMG can be made in the brief 20–30 ms interval between stimulus delivery and MEP onset, which is possible in recording conditions with little or no stimulus artefact. The procedure should prove to be important in conditions of varying EMG activity. Variability of corticospinal synaptic transmission is more difficult to control, because non-invasive measures of the state of motor cortical activity are not possible. Even if this was possible, the nature of synaptic transmission is inherently noisy (e.g. see Zucker et al. 2004). One can, nonetheless, insure constant stimulation coil placement and require subjects to concentrate on the task as mitigating measures. A comprehensive discussion of the factors that influence MEP variability can be found in Darling et al. (2006). Independent fluctuations in motoneuron pool and motor cortical excitability have been suggested to underlie MEP variability (Kiers et al. 1993). The lack of significant correlation between MEP amplitude and the mean level of background EMG suggests that the main source of variability, at least during tonic background contractions, is due to fluctuations of synaptic transmission at corticospinal terminals. This may, at least in part, be due to fluctuations of cortico-motoneuron recruitment from stimulus to stimulus.

In conclusion, one can nearly clamp the level of motoneuron pool activity to a desired level by asking subjects to maintain a prescribed level of muscle contraction, in which case MEP variability will mainly reflect inevitable fluctuations of corticospinal synaptic transmission and cortico-motoneuron recruitment.

## Epilogue

MEP amplitude is a sigmoid function of stimulus intensity and MEP variance is an inverted parabolic function of MEP amplitude. A mathematical model that explains these experimental results in neurophysiological terms was presented. Elaboration of the model was guided by the idea that simplification is often crucial for insight, as remarked by Wilson (1999) amongst others. Thus, a minimal mechanistic description of how an  $\alpha$ -motoneuron of given excitability and discharge threshold responds to synchronous but noisy synaptic inputs, such as TMS-evoked corticospinal volleys, was developed. This led to Eq. 4 relating discharge probability to mean input current that is central to the overall model. More complex motoneuron models that include a variety of intrinsic conductances and cable properties would not yield results which differ in any principal way from those presented. The distribution of motoneuron excitability within the pool was distributed according to a *pdf* that fits experimental findings. The results are largely independent of the exact nature of the *pdf*, as long as it is positively skewed and has a sigmoid *cdf*. The sigmoid nature of MEP amplitude as a function of stimulus intensity, the input–output curve, is due to the orderly recruitment of units along the *cdf*. The increasing size of MUAPs with recruitment order only changes the coefficients of the sigmoid, such as its scale. The gain change which occurs in going from rest to tonic motor activity is due to compression and up-scaling of the *pdf*. The inverted parabolic relation between MEP variance and MEP amplitude is due to the discharge variance characteristics of single units following the statistics of Bernoulli trials and the non-uniform nature of the Rayleigh *pdf*. The variance peaks near the median value of the distribution, where the density of motoneurons is greatest.

**Acknowledgements** This work was funded by the Canadian institutes of Health Research (CIHR) and in part by the Natural Sciences and Engineering Research Council of Canada (NSERC).

I thank Professors W.G. Darling and J.C. Rothwell for their comments and suggestions on a draft of the manuscript.

## References

- Capaday C (1997) Neurophysiological methods for studies of the motor system in freely moving human subjects. *J Neurosci Methods* 74:201–218. [https://doi.org/10.1016/s0165-0270\(97\)02250-4](https://doi.org/10.1016/s0165-0270(97)02250-4)
- Capaday C, Stein RB (1987) A method for simulating the reflex output of a motoneuron pool. *J Neurosci Methods* 21:91–104. [https://doi.org/10.1016/0165-0270\(87\)90107-5](https://doi.org/10.1016/0165-0270(87)90107-5)
- Capaday C, Lavoie BA, Barbeau H et al (1999) Studies on the corticospinal control of human walking. I. Responses to focal transcranial magnetic stimulation of the motor cortex. *J Neurophysiol* 81:129–139. <https://doi.org/10.1152/jn.1999.81.1.129>
- Darling WG, Wolf SL, Butler AJ (2006) Variability of motor potentials evoked by transcranial magnetic stimulation depends on muscle activation. *Exp Brain Res* 174:376–385. <https://doi.org/10.1007/s00221-006-0468-9>
- Devanne H, Lavoie BA, Capaday C (1997) Input-output properties and gain changes in the human corticospinal pathway. *Exp Brain Res* 114:329–338. <https://doi.org/10.1007/pl00005641>
- Devanne H, Cohen LG, Kouchtir-Devanne N, Capaday C (2002) Integrated motor cortical control of task-related muscles during pointing in humans. *J Neurophysiol* 87:3006–3017. <https://doi.org/10.1152/jn.2002.87.6.3006>
- Devore, J.L. (1987) Probability and Statistics for Engineering and the Sciences, 2nd edn. Brooks/Cole Publishing Company
- Dideriksen JL, Negro F, Enoka RM, Farina D (2012) Motor unit recruitment strategies and muscle properties determine the influence of synaptic noise on force steadiness. *J Neurophysiol* 107:3357–3369. <https://doi.org/10.1152/jn.00938.2011>
- Enoka RM (2008) Neuromechanics of human movement. Human Kinetics
- Ferguson GA (1976) Statistical analysis in psychology and education, 4th edn. McGraw-Hill Inc, New York
- Fuglevand AJ, Winter DA, Patla AE (1993) Models of recruitment and rate coding organization in motor-unit pools. *J Neurophysiol* 70:2470–2488. <https://doi.org/10.1152/jn.1993.70.6.2470>
- Gustafsson B, Pinter MJ (1984) An investigation of threshold properties among cat spinal alpha-motoneurons. *J Physiol* 357:453–483. <https://doi.org/10.1113/jphysiol.1984.sp015511>
- Hodgkin AL, Huxley AF (1952) A quantitative description of membrane current and its application to conduction and excitation in nerve. *J Physiol* 117:500–544. <https://doi.org/10.1113/jphysiol.1952.sp004764>
- Hunt CC (1955) Monosynaptic reflex response of spinal motoneurons to graded afferent stimulation. *J Gen Physiol* 38:813–852. <https://doi.org/10.1085/jgp.38.6.813>
- Julkunen P, Säisänen L, Hukkanen T et al (2012) Does second-scale intertrial interval affect motor evoked potentials induced by single-pulse transcranial magnetic stimulation? *Brain Stimulat* 5:526–532. <https://doi.org/10.1016/j.brs.2011.07.006>
- Keenan KG, Farina D, Merletti R, Enoka RM (2006) Influence of motor unit properties on the size of the simulated evoked surface EMG potential. *Exp Brain Res* 169:37–49. <https://doi.org/10.1007/s00221-005-0126-7>
- Kiers L, Cros D, Chiappa KH, Fang J (1993) Variability of motor potentials evoked by transcranial magnetic stimulation. *Electroencephalogr Clin Neurophysiol* 89:415–423. [https://doi.org/10.1016/0168-5597\(93\)90115-6](https://doi.org/10.1016/0168-5597(93)90115-6)
- Klein-Flügge MC, Nobbs D, Pitcher JB, Bestmann S (2013) Variability of human corticospinal excitability tracks the state of action preparation. *J Neurosci Off J Soc Neurosci* 33:5564–5572. <https://doi.org/10.1523/JNEUROSCI.2448-12.2013>
- Kouchtir-Devanne N, Capaday C, Cassim F et al (2012) Task-dependent changes of motor cortical network excitability during precision grip compared to isolated finger contraction. *J Neurophysiol* 107:1522–1529. <https://doi.org/10.1152/jn.00786.2011>
- Lavoie BA, Cody FW, Capaday C (1995) Cortical control of human soleus muscle during volitional and postural activities studied using focal magnetic stimulation. *Exp Brain Res* 103:97–107. <https://doi.org/10.1007/BF00241968>

- Pellicciari MC, Miniussi C, Ferrari C et al (2016) Ongoing cumulative effects of single TMS pulses on corticospinal excitability: an intra- and inter-block investigation. *Clin Neurophysiol* 127:621–628. <https://doi.org/10.1016/j.clinph.2015.03.002>
- Press WH, Flannery BP, Teukolsky SA, Vetterling WT (1986) *Numerical recipes: The art of scientific computing*. Cambridge University Press, Cambridge
- Rall W (1955a) Experimental monosynaptic input-output relations in the mammalian spinal cord. *J Cell Comp Physiol* 46:413–437. <https://doi.org/10.1002/jcp.1030460303>
- Rall W (1955b) A statistical theory of monosynaptic input-output relations. *J Cell Comp Physiol* 46:373–411. <https://doi.org/10.1002/jcp.1030460302>
- Rudomin P (1980) Information processing at synapses in the vertebrate spinal cord: presynaptic control of information transfer in monosynaptic pathways. In: *Information processing in the nervous system*. Raven Press, New York, pp 125–155
- Rudomin P, Dutton H (1969) Effects of conditioning afferent volleys on variability of monosynaptic responses of extensor motoneurons. *J Neurophysiol* 32:140–157. <https://doi.org/10.1152/jn.1969.32.2.140>
- Suckley JJ, Waters TJ, Tran M et al (2020) Randomising stimulus intensity improves the variability and reliability of the assessment of corticospinal excitability. *J Neurosci Methods* 342:108813. <https://doi.org/10.1016/j.jneumeth.2020.108813>
- Trappenberg TP (2002) *Fundamentals of computational neuroscience*. Oxford University Press
- Zucker RS, Kullmann DM, Schwarz TL (2004) *Release of neurotransmitters. From molecules to networks*. Elsevier Academic Press, Amsterdam, pp 197–235

**Publisher's Note** Springer Nature remains neutral with regard to jurisdictional claims in published maps and institutional affiliations.